

When Will Arctic Sea Ice Disappear?

Projections of Area, Extent, Thickness, and Volume

Francis X. Diebold

University of Pennsylvania

Glenn D. Rudebusch

Brookings Institution

Maximilian Göbel

University of Lisbon

Philippe Goulet Coulombe

University of Quebec at Montreal

Boyuan Zhang

University of Pennsylvania

March 9, 2022

Abstract: Rapidly diminishing Arctic summer sea ice is a strong signal of the pace of global climate change. We provide point, interval, and density forecasts for four measures of Arctic sea ice: area, extent, thickness, and volume. Importantly, we enforce the joint constraint that these measures must *simultaneously* arrive at an ice-free Arctic. We apply this constrained joint forecast procedure to models relating sea ice to cumulative carbon dioxide emissions and models relating sea ice directly to time. The resulting “carbon-trend” and “time-trend” projections are mutually consistent and predict an effectively ice-free summer Arctic Ocean by the mid-2030s with an 80% probability. Moreover, the carbon-trend projections show that global adoption of a lower emissions path would likely delay the arrival of a seasonally ice-free Arctic by only a few years.

Acknowledgments: For comments we thank, without implicating, the Penn Climate Econometrics Research Group and Walt Meier. For research assistance we thank Aaron Mora-Melendez, Jack Mueller, and Gladys Teng. All errors are ours alone.

Key words: Climate change, climate prediction, climate forecasting, carbon emissions, cryosphere

JEL codes: Q54, C51, C52, C53

1 Introduction

Understanding the climatic observational record (COR) is central to assessing the agreement (or lack thereof) between climate data and models – whether the climate scientists’ large-scale “global climate models” or the economists’ “integrated assessment models” of the climate-economy interaction. Understanding the COR can be facilitated via reduced-form econometric/statistical methods, which are designed to summarize data patterns (correlations) – that is, to “get the facts straight” – regardless of the deep causal climatic mechanisms generating the data.¹ Hence, determining whether various models “match the data” amounts to assessing whether they match the COR as embodied in econometric characterizations of trend, cycle, seasonality, volatility, structural change, and so on.

The COR has many diverse elements – such as temperature (means, extremes, variability, etc.) and extreme events (storms, floods, droughts, fires, etc.) – and these elements differ importantly at a granular spatial level. The Arctic region has emerged as a clear focal point for investigations of ongoing climate change. On the one hand, Arctic melting is a conspicuous *effect* of climate change, which has warmed the Arctic at least twice as quickly as the global average. In addition, the melting Arctic is a *cause* of additional future climate change, in part due to a “albedo” feedback amplification loop as the Arctic sea ice is replaced by darker open water. Along with global effects, the melting Arctic also has pervasive regional economic consequences. For example, less Arctic sea ice will reduce the cost of shipping, promote the extraction of polar natural resources, and expand tourism. Together, at a global and regional level, a melting Arctic will result in widespread and far-reaching economic impacts, opportunities, and risks (Alvarez et al., 2020).

Of course, given the importance of Arctic sea ice, there is a large literature examining and projecting its loss.² Large-scale climate models have been the source of much of the forward-looking sea ice analysis. These models attempt to capture the fundamental physical drivers of the earth’s climate with much geographic detail. Such structural models are invaluable for understanding climate variation; however, from a forecasting perspective, climate models have generally underestimated the amount of lost sea ice in recent decades (e.g., Stroeve et al., 2012 and Rosenblum and Eisenman, 2017). Of course, *statistical* projections of sea

¹The ability of reduced-form econometric/statistical methods to get the facts straight even with an incomplete understanding of the deep structure of climate dynamics is invaluable, because the deep structure of climate dynamics is indeed incompletely understood – witness the fifty or so different CMIP6 GCMs and their widely-differing projections, e.g. Notz (2020).

²Insightful overviews include Stroeve et al. (2012), Stroeve and Notz (2018), and Fox-Kemper et al. (2022).

ice are an obvious complementary approach. As a practical matter, parsimonious dynamic time series representations often produce forecasts that are at least as accurate as detailed structural models. Specifically, for forecasting Arctic sea ice, there is already some evidence that small-scale statistical models with no explicitly embedded physical science can have some success (Wang et al., 2016).

Therefore, we provide an econometric/statistical analysis of the long-run future evolution of Arctic sea ice. Of particular interest are probability assessments of the timing of an ice-free Arctic, an outcome with vital economic and climate consequences (Jahn et al., 2016). A key contribution of our analysis is that we take a multivariate approach to the various measures of Arctic sea ice. Specifically, we consider three aspects of pan-Arctic sea ice: surface coverage, thickness, and volume. In theory, these three measures of sea ice should be perfectly related. Volume would equal the product of surface coverage and thickness, so modeling any two would imply a specification for the third. In practice, however, each sea-ice indicator is based on a blend of the pure observations and model interpretations and interpolations. As a result, measurement differences and errors introduce discrepancies between the various indicators and drive wedges between them, even if the amount of measurement error has generally diminished over time as observational and modeling methods have improved. Thus, the various measures of sea ice are not perfectly related, and it is beneficial to consider all of them.

We characterize September Arctic sea ice – the month with the least seasonal ice – as a time series process and examine its likely future path towards ice-free conditions with continued global warming. In particular, we focus on estimating the timing of the first ice-free September, exploring both a literally ice-free Arctic (IFA) and an effectively or nearly ice-free Arctic (NIFA).³ We model sea ice area, extent, thickness, and volume, and we implement multivariate models that constrain them to reach zero simultaneously. We anchor our analysis on area, sequentially considering pairwise blends of area with each of the other indicators. The area-extent pair is essentially based on only observed data; the area-thickness pair integrates the two key indicators characterizing sea ice; and the area-volume pair is closest to an all-indicator analysis that incorporating area, thickness, and extent.

We implement our constrained joint forecasting procedure in “carbon-trend” models that relate sea ice to cumulative carbon dioxide emissions, allowing us to condition our forecasts on various emissions scenarios. We also check our carbon-trend results against similarly-

³We follow the usual convention and define NIFA as sea ice coverage of less than 10^6 km^2 . The common use of NIFA reflects the hypothesized persistence of thick sea ice clinging to northern coastlines – notably in Greenland and Canada – despite an open Arctic ocean (Wang and Overland, 2009).

constrained “time-trend” models that relate sea ice simply to time. Finally, we verify the consistency of the two approaches, and we use them to make probabilistic forecasts of the arrival years of NIFA and IFA.

There is of course a huge literature on measurement and modeling of declining Arctic sea ice extent and area. Insightful overviews include Stroeve et al. (2012) and Shalina et al. (2020a). There are also literatures on measurement and modeling of declining thickness and volume; see Stroeve and Notz (2018) and Shalina et al. (2020b). We will subsequently have more to say about the literature and how our results relate to it. For now, however, we emphasize again that our multivariate modeling of area, extent, thickness, and volume – respecting in particular the fact that if and when they vanish, they must vanish simultaneously – sets us apart.

We proceed as follows. In section 2, we introduce our four sea ice indicators. In section 3, we model and forecast the indicators using regressions on cumulative carbon emissions (“carbon trends”), producing point and interval forecasts. In section 4 we provide a major robustness check by modeling and forecasting using direct trend regressions instead (“time trends”), assessing the consistency of the carbon-trend and time-trend forecasting approaches. In section 5 we use both approaches to provide full probabilistic forecasts of the two objects of ultimate interest: the arrival years of IFA and NIFA. In section 6 we provide a second major robustness check by redoing most of the carbon-trend analysis using an alternative carbon measure, atmospheric CO₂ concentration, assessing the consistency of the two carbon-trend versions. We conclude in section 7.

2 Measures of Arctic Sea Ice

We consider three key aspects of Arctic sea ice: surface coverage, thickness, and volume. Our analysis focuses on the seasonal minima for these indicators, specifically, September monthly average data at a pan-Arctic scale (for details, see Appendix A).

2.1 Area and Extent

Arctic sea ice surface coverage has been well measured using satellite-based passive microwave sensing since late 1978. To do this, the Arctic is divided into a grid of cells, and for each cell, satellite sensors measure the amount of reflected solar radiation. This reflected energy varies from cell to cell depending on the relative cell coverage of sea ice and open water, as the latter absorbs more radiation. The resulting measured “brightness” is converted into a

fractional measure of sea-ice “concentration” for cell i at time t , denoted $c_{i,t}$. The individual $c_{i,t}$ are then aggregated into two standard and somewhat different measures of overall sea-ice coverage.

The first of these, “sea-ice area” (SIA), sets measured concentration in each cell to zero if it is below .15 and retains the satellite-recorded value otherwise:

$$c_{i,t}^{SIA} = \begin{cases} 0, & \text{if } c_{i,t} \leq .15 \\ c_{i,t}, & \text{otherwise.} \end{cases} \quad (1)$$

All grid cell areas are then multiplied by $c_{i,t}^{SIA}$, and their weighted sum over the entire Arctic is denoted SIA_t . As a result, SIA is the measured coverage of all Arctic grid cells with at least 15 percent sea-ice concentration.

The second measure of coverage, “sea-ice extent” (SIE), also sets measured concentration below .15 to zero but otherwise adjusts it upward to full coverage, or 1:

$$c_{i,t}^{SIE} = \begin{cases} 0, & \text{if } c_{i,t} \leq .15 \\ 1, & \text{otherwise.} \end{cases} \quad (2)$$

In this case, all grid cell areas are multiplied by $c_{i,t}^{SIE}$, and their weighted sum is total Arctic SIE_t . Thus, SIE is the total area of all of the ocean grid cells that are measured to have at least 15% sea-ice coverage.

The up-rounding in the construction of SIE serves as a bias correction to offset satellite sensors’ tendency to mistake shallow pools of sea-ice surface melt for open sea.⁴ There are costs and benefits of such a bias correction, and both SIA and SIE are widely employed in research and forecasting. We will examine both, using September monthly average SIA and SIE data from 1979 to 2021 from the National Snow and Ice Data Center (NSIDC).

The up-rounding in the construction of SIE also implies that by definition $SIE \geq SIA$, and indeed, in the historical data, SIE has been substantially higher than SIA . For our analysis, the crucial definitional constraint is that these two measures of sea ice coverage can only equal zero under the same condition, that is, when *all* Arctic grid cells have no more than fifteen percent coverage ($c_{i,t} \leq .15$ for all i). In that case, the two measures will be equivalent, so $SIA = SIE = 0$. This constraint that both indicators must reach zero at the same time will be the crucial timing restriction that allows us to construct a joint projection of pan-Arctic September SIA and SIE .

⁴See <https://www.ncdc.noaa.gov/monitoring-references/dyk/arctic-ice> for details.

2.2 Thickness and Volume

Our third sea-ice indicator is thickness, denoted SIT . Sea-ice thickness – the distance between the ocean underneath and any snow coverage above the ice – is challenging to measure but provides a fuller understanding of sea ice conditions.⁵ In the past, data on sea-ice thickness have been obtained via a variety of methods including submarine records, ocean floor buoys, bore holes, helicopter and sled surveys, and satellite measures, but these sources have varying accuracy and availability by time and location. A popular alternative to these disparate thickness measures is produced by the Pan-Arctic Ice-Ocean Modeling and Assimilation System (PIOMAS) from the University of Washington’s Polar Science Center (Zhang and Rothrock, 2003). The PIOMAS thickness indicator incorporates (or assimilates) data such as the NSIDC sea-ice concentration measure as well as atmospheric information such as wind speed and direction, surface air temperature, and cloud cover. However, the PIOMAS data are importantly driven by an ocean and sea ice physical model that characterizes how sea-ice thickness evolves over location and time in response to dynamic and thermodynamic forcing and mechanical redistribution such as ridging. That is, the PIOMAS thickness data are largely a model construct, although they have been largely validated against the available observational data. For example, Selyuzhenok et al. (2020), building on Schweiger et al. (2011), report that the spatial pattern of PIOMAS ice thickness agrees well with observations derived from in situ and satellite data, and Labe et al. (2018) note that decadal trends in thickness appear realistically reproduced. Surveys that reach a similar conclusion include Leppäranta et al. (2020, section 8.4) and Shalina et al. (2020b, section 5.6).

Our fourth sea-ice indicator is volume, SIV , which is also supplied via the model-based PIOMAS measurement. Specifically, across a grid of cells, this series combines the PIOMAS thickness and the sea-ice coverage data to produce sea-ice volume cell by cell. Of course, in theory, volume, which represents the entire mass of sea ice, should be the most comprehensive indicator of Arctic sea ice. On the other hand, SIV , which is produced as the product of surface coverage and thickness, inherits measurement error from both of those series and appears to be subject to the most uncertainty in measurement.

As noted above, our joint estimation approach relies on a simultaneous zero-ice constraint. The two sea-ice coverage series, SIA and SIE , share data sources and definitions that effectively hard-wire or force a simultaneous ice-free Arctic. A similar exact relation-

⁵See, for example, Bunzel et al. (2018), Chevallier et al. (2017), Shalina et al. (2020b), Notz (2020), and Zygmuntowska et al. (2014).

ship is less assured for thickness and volume as these depend on model-based imputations. Furthermore, SIT and SIV do not impose the 15% cutoff used in SIA and SIE , which in theory could lead to later ice-free dates for thickness and volume (the opposite of what we will uncover below). However, given that *all* four indicators depend on the amount of sea-ice coverage, it is likely that SIA , SIE , SIT , and SIV will all reach zero very closely in time if not simultaneously, and we will assess the imposition of that constraint in estimation of sea-ice dynamics.

3 Linear Carbon-Trend Models, Fits, and Forecasts

Here we explore the empirical relationships between the four Arctic sea-ice indicators and the level of cumulative anthropogenic industrial CO_2 emissions. We then use these representations to forecast the likely progression of a melting Arctic and, specifically, the years of first IFA and NIFA.

3.1 The Carbon-Trend Model

Various researchers – including Johannessen (2008), Notz and Stroeve (2016), and Stroeve and Notz (2018) – have identified a linear empirical relationship between observed Arctic sea ice area and atmospheric CO_2 cumulative emissions. This linear carbon-trend relationship, which fits remarkably well in the observed data, can be expressed as:

$$SIA_t = a + b CO2_t + \varepsilon_t, \quad (3)$$

where SIA_t is sea ice area, $CO2_t$ is cumulative anthropogenic CO_2 emissions since 1850, and ε_t represents deviations from the linear fit. The regression intercept, a , calibrates the level of sea ice coverage, and the slope, b , provides a measure of the carbon-climate response of Arctic sea ice, or the “Arctic sea-ice climate sensitivity.” A negative value for b captures the diminishing coverage of Arctic sea ice as greenhouse gases accumulate in the atmosphere. Equation (3) also can be used to characterize the occurrence of first IFA in terms of $CO2$. In particular, the level of cumulative emissions consistent with the first occurrence of an ice-free Arctic ($SIA_t = 0$) occurs when $CO2_t = -a/b$.

The “univariate” representation (3) has typically been used to fit and forecast a single sea-ice indicator – either sea-ice area or extent. We will generalize this analysis to consider thickness and volume as well. More importantly, we will also introduce a joint modeling

strategy that allows two or more sea-ice indicators to be modeled together. Such a representation combines indicators using a simultaneous zero-ice constraint. For example, for two indicators, the “bivariate” linear carbon trend model with a “common first IFA” constraint is given by

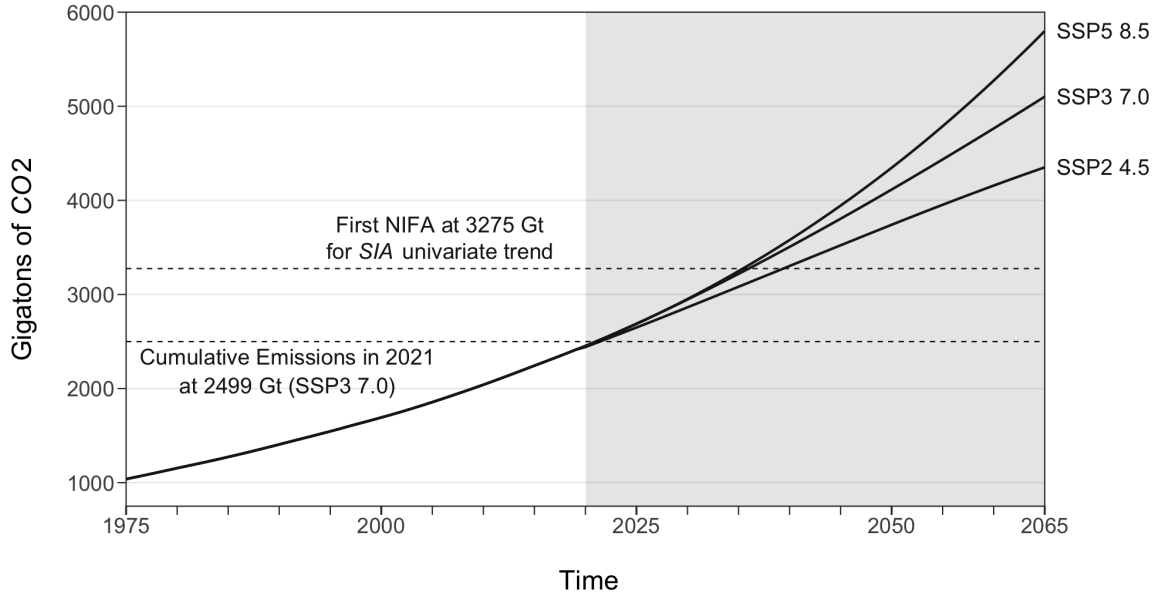
$$\begin{aligned} x_t &= a^x + b^x CO2_t + \varepsilon_t^x \\ y_t &= a^y + \frac{a^y b^x}{a^x} CO2_t + \varepsilon_t^y, \end{aligned} \tag{4}$$

where x_t and y_t are two sea-ice indicators. This regression model has jointly constrained slopes and intercepts so that $x_t = y_t = 0$ at the same level of $CO2_t$ and can be estimated via non-linear least squares. Like the univariate equation (3), the bivariate system (4) can be used to characterize a first (simultaneous) IFA in terms of $CO2$ – that is, a carbon level for a seasonal ice-free Arctic.

For our bivariate empirical analysis with (4), we always set x_t to SIA_t and y_t to one of the other sea ice indicators (SIE_t , SIT_t , or SIV_t). Of course, the first-IFA constrained model can be generalized to more than two indicators. Indeed, we have applied it to 3- and 4-variable sets of our sea ice indicators and obtained similar empirical results to those reported below.⁶ However, our focus here is on the three bivariate combinations: $SIA+SIE$, $SIA+SIT$, and $SIA+SIV$.

Each indicator pair brings additional information to the estimation of the first IFA year by incorporating additional indicators with SIA , which provides a common benchmark for comparing results. In addition, each pair has idiosyncratic characteristics that provide useful differentiation. The $SIA+SIE$ pair is only one that is based on data that are essentially directly observed, and these two indicators also share a clear-cut zero-ice constraint by definition. However, this pair is limited to only sea ice coverage, while the other combinations account for thickness as well. The $SIA+SIT$ pair integrates the two key elements necessary for measuring sea ice, but again, SIT is a model-processed measure that has greater measurement error. The $SIA+SIV$ pair combines area with the most comprehensive measure of sea ice, but again, at a likely cost of measurement accuracy.

Figure 1: Cumulative Carbon Emissions Scenarios



Notes: We show historical data and three projected scenarios for cumulative global carbon dioxide emissions, measured in 10^9 tons (gigatons, Gt). The historical period (to 2019) is unshaded, and the out-of-sample period is shaded. The lower dashed line denotes current emissions, and the upper dashed line provides our estimate of CO_2 at first IFA for the *SIA* univariate carbon-trend specification.

3.2 Carbon Emissions Data

Our CO_2 data (measured in gigatons, Gt) are shown in Figure 1. They are based on Rogelj et al. (2021) and served as input to the IPCC AR6 report (Allan et al., 2022).⁷ The data in the unshaded region (1975-2019) are based on historical observations of cumulative anthropogenic carbon emissions since 1850 (from all energy, industrial, and land use sources). The shaded region shows three alternative standard emissions scenarios, which are denoted SSP2 4.5 (medium), SSP3 7.0 (medium-high), and SSP5 8.5 (high).⁸ The SSP scenarios in Figure 1 are distinguished by the amount of progress made in reducing further CO_2 emissions as shown by the variation in their upward curvature. While some of our analysis will use the SSP3 7.0 scenario as a baseline, we will also show that our results are robust to the use of the other scenarios.

⁶Subtleties also arise with 3- and 4-variable systems, such as additional potentially relevant restrictions among indicators, as when, for example, *SIV* is at least the approximate product of *SIE* and *SIT*.

⁷See Appendix A for details.

⁸See, for example, Arias (2022).

3.3 Carbon-Trend Fits and Forecasts in Ice-Carbon Space

Fitted and forecast linear carbon-trends for all four Arctic sea-ice indicators are shown in Figure 2, each panel of which graphs a pair of sea ice measures against the cumulative emissions series CO_2 . Unconstrained univariate results appear in the left panels, and common-IFA constrained bivariate results for various pairs of indicators appear in the right panels. The historical sea-ice data from 1979 to 2021 are in the unshaded sample and the shaded sample shows projections.⁹ The black irregular lines show SIA (measured in 10^6 km^2) versus CO_2 , and the blue, red, and green irregular lines are for SIE , SIT , and SIV (measured in 10^6 km^2 , m, and 10^3 km^3 , respectively). These various standard units of measurement are such that the pairs of SIA , SIE , SIT , and SIV can be plotted conveniently together in the various panels of Figure 2, but this convenience is irrelevant for our results. Trend regression coefficient estimates depend on the choice of measurement units, but, crucially, the implied estimates of our key objects of interest, namely, the extrapolated years of the first ice-free Arctic, do not depend on these units.

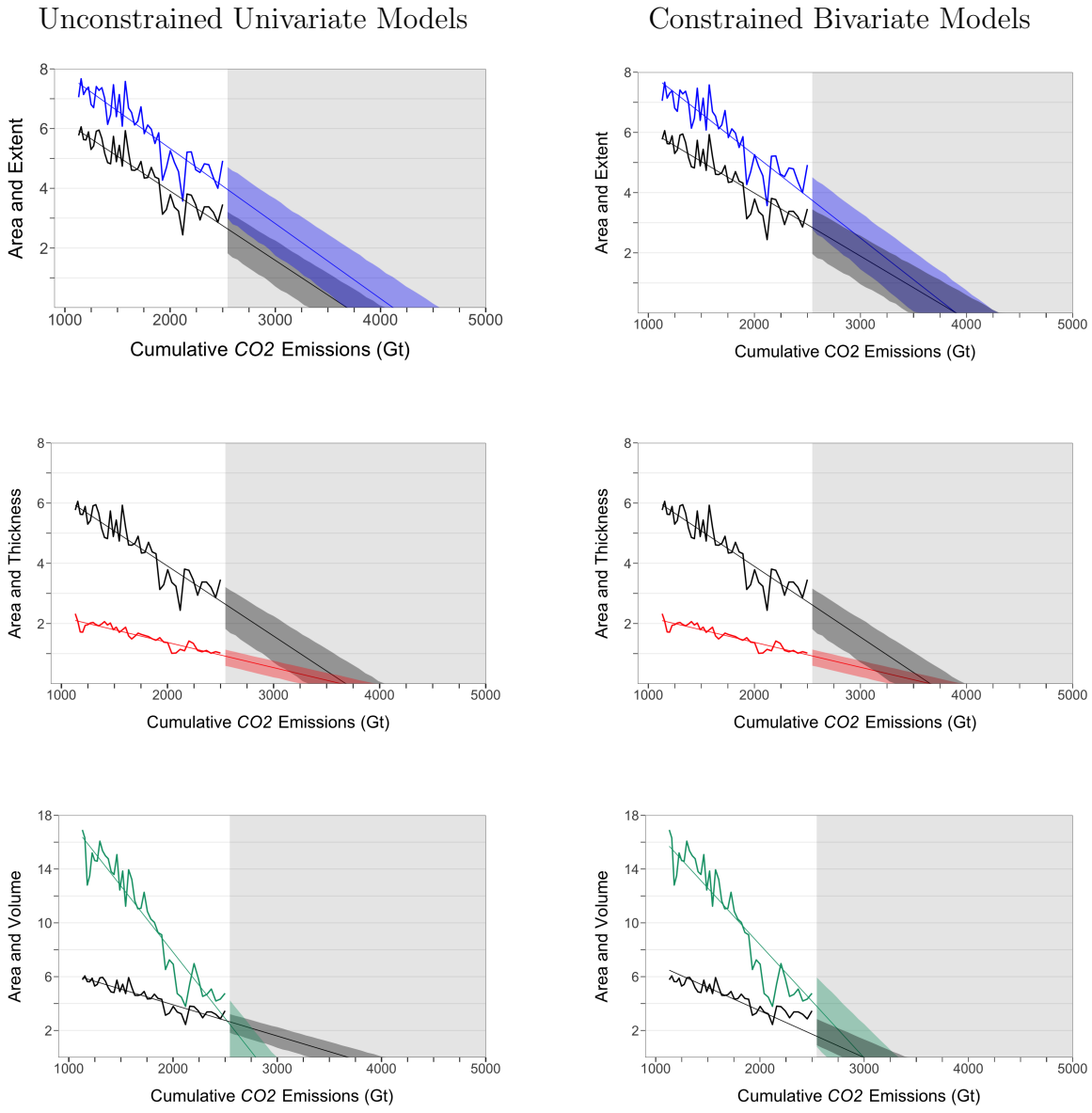
In Figure 2, linear carbon trends, again colored black, blue, red, and green for SIA , SIE , SIT , and SIV , are fitted to the data in the unshaded sample. Their fit illustrates how well the linear regressions capture the relationships between the sea-ice indicators and cumulative emissions. For each measure, the historical data cluster quite tightly around the fitted carbon trends. This remarkably robust linearity has been noted for sea-ice area in the literature (e.g., Notz and Stroeve, 2016), and here we generalize this result to other measures. In percentage terms, Arctic sea-ice coverage and thickness have trended downward at a similar rate, with SIE , SIA , and SIT falling by about 50% over the sample. When combined, these declines account for the 75% drop in SIV over the sample.

In the shaded regions of Figure 2, the carbon trends are extrapolated beyond the historical sample until the arrival of an ice-free Arctic. The unconstrained univariate column reveals that projected carbon at first IFA is higher for SIE than for SIA , slightly lower for SIT , and notably lower for SIV . Comparing the univariate and constrained bivariate columns of Figure 2, one sees that imposition of the simultaneous first-IFA constraint changes the slopes of the fitted and extrapolated carbon trends. This is consistent with the fact that for each pair of indicators, the common constrained first-IFA carbon levels lie between the two unconstrained first-IFA carbon levels.

The qualitative insights from Figure 2 are detailed in Table 1. The estimated Arctic

⁹These regressions use the historical CO_2 data from 1979 to 2019 and two additional years of data from the SSP3 7.0 scenario to complete the sample.

Figure 2: September Arctic Sea Ice Indicators:
Estimated Linear Carbon Trends in Ice-Carbon Space Under SSP3 7.0



Notes: Each panel displays a pair of sea ice indicators graphed against CO_2 (cumulative global carbon dioxide emissions, measured in Gt). We show extent in blue (measured in 10^6 km^2), area in black (measured in 10^6 km^2), thickness in red (measured in m), and volume in green (measured in 10^6 km^3). In the univariate column, we show linear carbon-trend fits and forecasts based on Equation (3). In the bivariate column, we show linear carbon-trend fits and forecasts constrained to reach zero simultaneously, based on Equation (4). The historical sample period (unshaded) is 1979-2021, and the forecast intervals obtained by simulation have 90% coverage.

Table 1: September Arctic Sea Ice Indicators:
Linear Carbon Trend Estimates and Projections (Under SSP3 7.0)

Model	\hat{b}	R^2	First IFA		First NIFA (Area)	
			$CO2$ (Gt)	year	$CO2$ (Gt)	year
Unconstrained Univariate Models						
Area	-0.23 (0.02)	0.83	3,684	2043	3,275	2036
Extent	-0.25 (0.02)	0.80	4,179	2051		
Thickness	-0.08 (0.01)	0.86	3,684	2043		
Volume	-0.98 (0.05)	0.90	2,842	2028		
Constrained Bivariate Models						
Area	-0.21 (0.01)	0.82	3,928	2047	3,448	2039
Extent						
Area	-0.24 (0.01)	0.83	3,684	2043	3,275	2036
Thickness						
Area	-0.35 (0.02)	0.61	3,000	2031	2,740	2026
Volume						

Notes: We estimate linear carbon-trend models for *SIA*, *SIE*, *SIT*, and *SIV* from 1979 to 2021. The top panel reports shows univariate models for each indicator, and the bottom panel shows first IFA constrained bivariate models for *SIA* paired with *SIE*, *SIT*, or *SIV*. We report parameter estimates, R^2 's, and projected carbon levels and years at first IFA and first NIFA (the latter for *SIA* only). The first IFA and NIFA years are based on the time path under the SSP3 7.0 scenario. Throughout, standard errors appear in parentheses. The b estimates and standard errors have been multiplied by 100.

climate sensitivities (\hat{b} 's) are all negative and highly statistically significant, and all R^2 values are above .80. The univariate projected first-IFA carbon levels for *SIA*, *SIE*, *SIT*, and *SIV* are 3684 Gt, 4179 Gt, 3684 Gt, and 2842 Gt, respectively. When *SIA* is modeled jointly with *SIE*, *SIT*, and *SIV*, the bivariate constrained projected first-IFA carbon levels are 3928 Gt, 3684 Gt, and 3000 Gt. That is, the bivariate first-IFA carbon levels are higher or lower than the univariate estimate depending on which additional indicator is blended with *SIA*. Note that the bivariate constrained blending of *SIA* with the other indicators reduces the range of the projected first-IFA carbon levels; the univariate range is 4179–2842=1337 Gt, whereas the constrained bivariate range is 3928–3000=928 Gt.

While our bivariate common first-IFA constraint assumes the joint occurrence of a zero-ice event, the literature has often focused on the occurrence of an “effectively” ice-free Arctic, or NIFA, defined as an *SIA* or *SIE* level of 1 million km² or less. This definition reflects the view that certain coastal regions may retain small amounts of landfast sea ice even after the open Arctic Sea is ice free (Wang and Overland, 2009). However, the intractability of melting landfast ice remains an open issue of research, and there is much uncertainty about how resilient such a circumscribed “Last Ice” refuge will be to further warming (Cooley et al., 2020; Mudryk et al., 2021; Schweiger et al., 2021). Reflecting this uncertainty, while we also consider the usual definition of a nearly ice-free Arctic (10⁶ km²) for *SIA* and *SIE*, we do not account for any possible structural shift in near-zero sea-ice dynamics. Accordingly, Table 1 reports the projected first-NIFA carbon levels for *SIA*. For *SIT* or *SIV*, there are no similar definitions of effectively ice-free levels in the literature, so we concentrate on the occurrence of *SIA* first NIFA. Of course, any first-NIFA carbon level is lower than the associated first-IFA level, but the precise difference depends on the indicator(s) examined and model used (univariate vs. bivariate). The univariate projected *SIA* first-NIFA carbon level is 3275 Gt. It matches the constrained bivariate *SIA+SIT* *SIA* first-NIFA projection, and it is a little higher than that for *SIA+SIV*, and a little lower than that for *SIA+SIE*. The range of the first-NIFA carbon level projections is 3448–2740=708 Gt.

The “carbon budget” is a popular concept used to assess such carbon levels. The carbon budget is the difference between the *current* cumulative emissions level and the level associated with some event. For example, a recent estimate of the carbon budget – the remaining amount of CO₂ that can be emitted – to avoid exceeding the Paris Agreement’s 1.5°C global temperature target was 440 Gt (Matthews et al., 2021). Assuming a 2021 CO₂ value of 2499 Gt, our estimate of the Arctic carbon budget of additional future anthropogenic CO₂ emissions until the likely occurrence of a nearly ice-free Arctic is 776 Gt of CO₂ for the uni-

variate SIA and bivariate $SIA + SIT$ models (the difference between the dashed horizontal lines in Figure 1). The level is slightly higher or lower for the other model pairs.

Finally, although we have thus far discussed only point forecasts, we also provide simulation-based 90% interval forecasts in Figure 2, shown as shaded regions around the point forecasts.¹⁰ The intervals are generally quite narrow, despite their appropriate widening as the projection horizon lengthens, and we will provide a more detailed discussion of uncertainty below.

3.4 Carbon-Trend Fits and Forecasts in Ice-Time Space

The monotonically increasing carbon levels embedded in the historical and SSP scenarios of Figure 1 allow us to translate carbon-trend representations like (3) (in ice-carbon space) into time-trend representations (in ice-time space). In particular, the one-to-one SSP scenario mappings allow us to translate the first IFA/NIFA carbon level projections into projected first IFA/NIFA *years*.

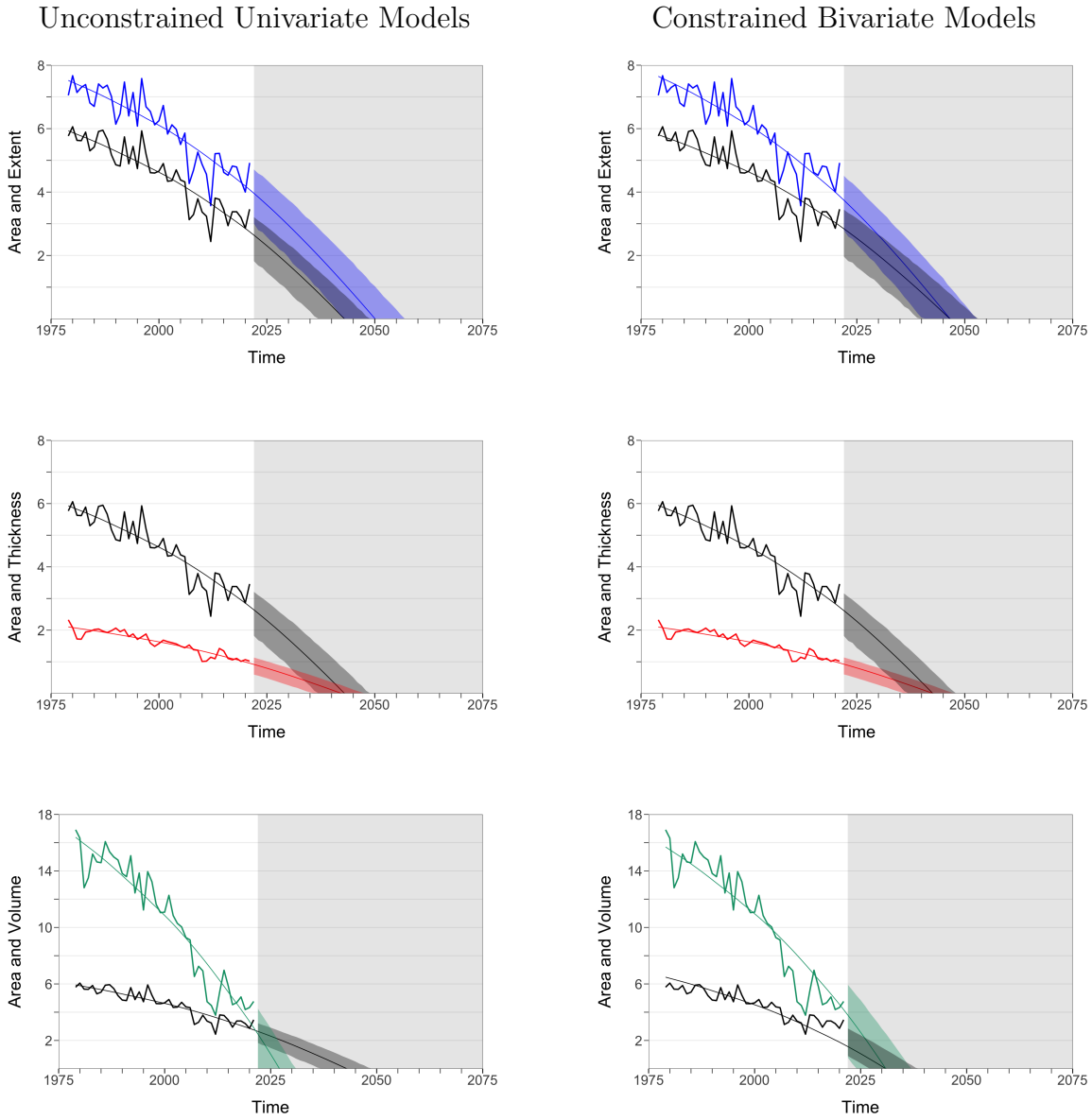
Moreover, the curvature of the SSP scenarios produces a curvature in the time trends implied by the linear carbon trends. For example, because the SIA is linearly related to CO_2 and the SSP scenarios used to convert carbon trends into time trends are nonlinear, the implied SIA time trend will be nonlinear. Furthermore, with the carbon scenarios increasing over time at increasing rates, the implied sea-ice time trends will be decreasing at increasing rates.

The implied fitted and forecasted nonlinear time trends are shown in Figure 3, the format of which parallels that of Figure 2. The implied time trends are obtained by running the fitted carbon trends of Figure 2 through the (inverse) emissions schedule SSP3 7.0 of Figure 1. Accordingly, each carbon level in ice-carbon space yields a corresponding time in ice-time space. For example, as discussed earlier, our univariate estimate of carbon at first NIFA is 3275 Gt. As seen by following the upper dashed horizontal line in Figure 1 (and as recorded in Table 1), a cumulative carbon level of 3275 translates under SSP3 7.0 into a first NIFA year of 2036.

Table 1 contains implied projected first-IFA and first-NIFA years. The univariate projected SIA first-IFA year is 2043, and the corresponding bivariate constrained projected first-IFA years are 2047, 2043, and 2031, depending on whether SIA is modeled jointly with SIE , SIT , or SIV , respectively. The range of univariate projected first-IFA years is 2051–

¹⁰The interval forecasts are obtained from 1000 bootstrap simulations, and they account for both parameter estimation uncertainty and disturbance uncertainty. For details see Appendix B.

Figure 3: September Arctic Sea Ice Indicators:
Estimated Linear Carbon Trends in Ice-Time Space Under SSP3 7.0



Notes: Each panel displays a pair of sea ice indicators graphed against time. We show extent in blue (measured in 10^6 km^2), area in black (measured in 10^6 km^2), thickness in red (measured in m), and volume in green (measured in 10^6 km^3). In the univariate column, we show linear carbon-trend fits and forecasts based on Equation (3), converted from ice-carbon space to ice-time space. In the bivariate column, we show linear carbon-trend fits and forecasts constrained to reach zero simultaneously, based on Equation (4), and again converted from ice-carbon space to ice-time space. The historical sample period (unshaded) is 1979-2021, and the forecast intervals obtained by simulation have 90% coverage.

2028=23 years, and the constrained bivariate range is 2047-2031=16 years. Table 1 also reports projected *SIA* first-NIFA years. The univariate projected *SIA* first-NIFA year is 2036. This date matches the constrained bivariate projected *SIA+SIT* first-NIFA year and is a little later and sooner than those for *SIA+SIV* and *SIA+SIE*, respectively. The range of the projected first-NIFA years is 2039-2026=13 years. Across all univariate and bivariate specifications, the average *SIA* first-NIFA data is 2034, so the occurrence of an effectively ice-free Arctic is clearly projected to occur fairly soon.

Finally, as we will describe in detail below, our first-IFA and first-NIFA dates are robust to the emissions scenario used. We have emphasized the mid-high SSP3 7.0 emissions scenario as a plausible baseline, but other scenarios provide similar dates because first NIFA occurs relatively rapidly before the carbon levels in the various scenarios can diverge. This can be seen immediately in Figure 1, where the horizontal line at 3275 Gt carbon cuts all three SSP schedules at nearly-identical times. Indeed moving to the mid-emissions SSP2 4.5 schedule produces only a small increase in the estimated first-NIFA year. That is, our results indicate that global adoption of a somewhat lower emissions path would likely delay the arrival of a seasonally ice-free Arctic by only a few years.

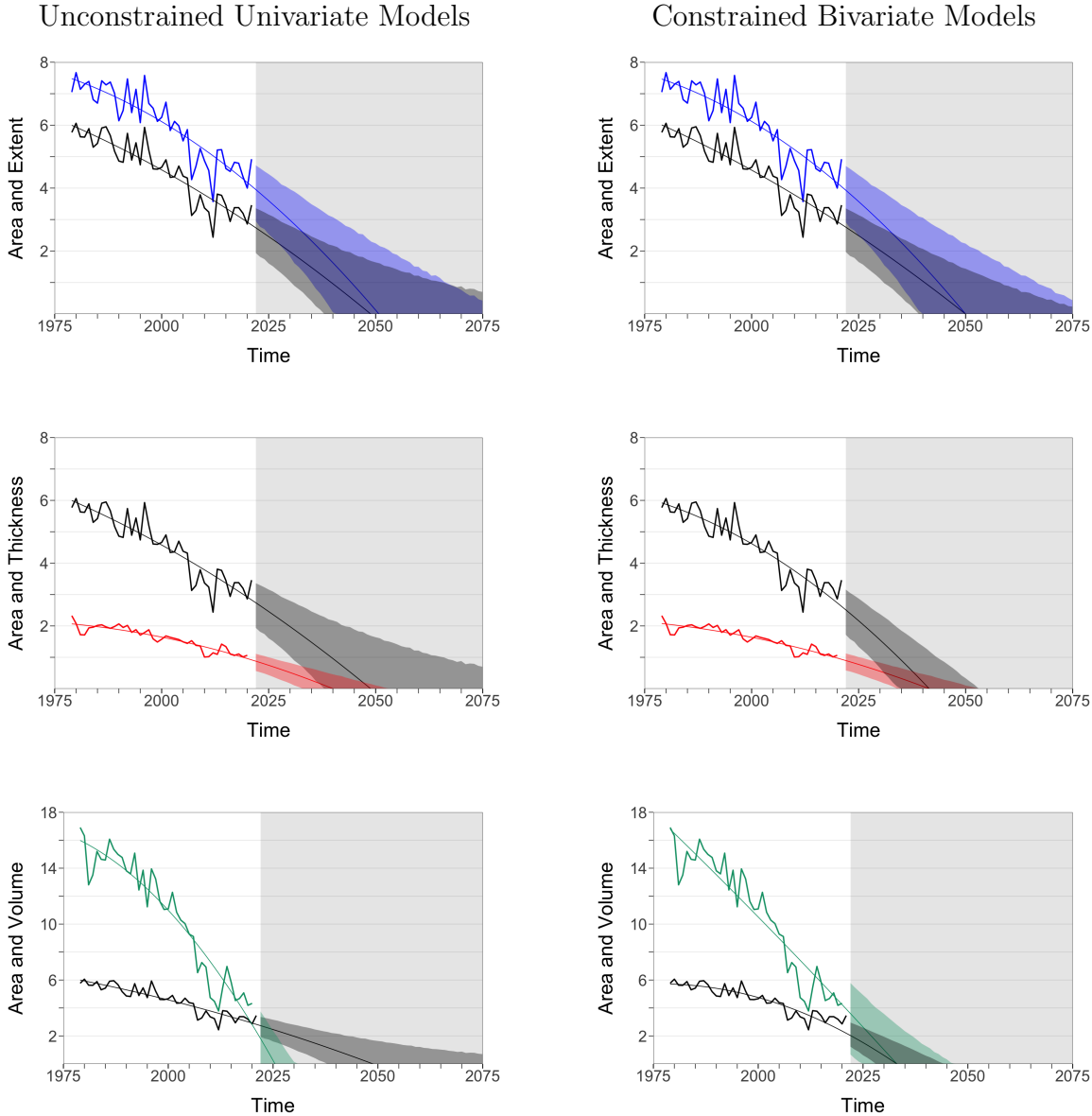
4 Quadratic Time-Trend Models, Fits, and Forecasts

In the previous section, we focused on the physical science connection between higher cumulative CO₂ amounts and melting Arctic ice, implicitly recognizing that higher greenhouse gas concentrations raise global surface temperatures and lead to melting ice. Remarkably, a simple linear regression appeared adequate, based on the past forty years, for forecasting CO₂ at first IFA and NIFA. We then used the leading SSP emissions scenarios to convert the forecasted sea-ice paths from ice-carbon space to ice-time space. That is, we ultimately forecasted the path and pattern of *SIA* diminution over time, and in particular, the years of first IFA and first NIFA. The nonlinear SSP paths converted the linear carbon trend into a nonlinear implied time trend, decreasing at an increasing rate.

As a first and major robustness check, we now compare the time trends obtained from the ice-carbon relationship to deterministic polynomial trends fit directly to *SIA*, as in Diebold and Rudebusch (2022b). In particular, we allow for the relevant ice-time nonlinearity by allowing for quadratic time effects. In the univariate approach, we use

$$SIA_t = a^x + b^x TIME_t + c^x TIME_t^2 + \varepsilon_t^x \quad (5)$$

Figure 4: September Arctic Sea Ice Indicators:
Estimated Quadratic Time Trends



Notes: We show extent in blue (measured in 10^6 km^2), area in black (measured in 10^6 km^2), thickness in red (measured in m), and volume in green (measured in 10^6 km^3). In the univariate column, we show direct quadratic time-trend regression fits and forecasts, based on Equation (5). In the bivariate column, we show direct quadratic time-trend regression fits and forecasts constrained to reach zero simultaneously, based on Equation (6). The historical sample period (unshaded) is 1979-2021, and the projection intervals obtained by simulation have 90% coverage.

where SIA_t is sea ice area, $TIME$ is a time trend dummy, and ϵ_t represents deviations from trend. Similarly, in the bivariate approach we use

$$x_t = a^x + b^x TIME_t + c^x TIME_t^2 + \varepsilon_t^x$$

$$y_t = a^y + b^y TIME_t + c^y TIME_t^2 + \varepsilon_t^y,$$

where x_t is SIA_t and y_t is one of the other sea ice indicators (SIE_t , SIT_t , SIV_t). Linearity of course emerges as a special case.

In our flagship constrained bivariate approach, we move to the equivalent root form of the quadratic system,

$$x_t = (\alpha^x - \beta^x TIME_t) (1 - \gamma^x TIME_t) + \varepsilon_t^x \quad (6)$$

$$y_t = (\alpha^y - \beta^y TIME_t) (1 - \gamma^y TIME_t) + \varepsilon_t^y,$$

where the roots of the x trend are $1/\gamma^x$ and α^x/β^x , and the roots of the y trend are $1/\gamma^y$ and α^y/β^y . Imposing the common first-IFA constraint (i.e., both trends reach zero simultaneously) amounts to constraining the two quadratics to have a common root, $\gamma^x = \gamma^y = \gamma$, which can immediately be done in a joint estimation of the two quadratic trends.¹¹

The fitted direct quadratic time trends are shown in Figure 4. The point forecast paths are reassuringly similar to those of the carbon-implied time trends in Figure 3. The interval forecast paths are wider, however, than for carbon-implied time trends. This is appropriate and expected, because the carbon-implied time trends of Figure 3 *assume* the amount of curvature via an assumed SSP path on which they condition, whereas the direct time trends of Figure 4 *estimate* the curvature, which is challenging. The extra parameter estimation uncertainty then translates into wider projection intervals. Put differently, the carbon-implied trends provide forecasts *conditional* on a particular assumed SSP scenario, whereas the directly-fitted time trends provide *unconditional* business-as-usual forecasts. Neither is “better” than the other; rather, they simply answer different but closely related questions, and both are useful, but the uncertainty associated with the directly-fitted time trends is naturally greater.

Parameter estimates for both the unconstrained univariate and constrained bivariate direct quadratic trends are highly statistically significant, and all R^2 ’s are above .8. The key bivariate projected first-NIFA years are 2041, 2037, and 2031, for $SIA+SIE$, $SIA+SIT$,

¹¹That is, in the joint regression, $a^i = \alpha^i$, $b^i = -\beta^i - \alpha^i\gamma$, and $c^i = \beta^i\gamma$, for $i = x, y$.

Table 2: September Arctic Sea Ice Indicators:
Probability Distributions of *SIA* First September NIFA Years

	Mean	Median	Mode	Std	Skew	Kurt	5%	20%	80%	95%
<u>SSP5 8.5</u>										
<i>SIA+SIE</i>	2035	2036	2036	3.41	-0.31	2.76	2029	2032	2038	2040
<i>SIA+SIT</i>	2033	2033	2034	2.81	-0.44	2.99	2028	2031	2035	2037
<i>SIA+SIV</i>	2025	2025	2025	2.04	0.48	2.87	2022	2023	2027	2029
<u>SSP3 7.0</u>										
<i>SIA+SIE</i>	2036	2036	2037	3.69	-0.24	2.70	2029	2032	2039	2041
<i>SIA+SIT</i>	2033	2033	2034	2.99	-0.36	2.93	2028	2031	2036	2038
<i>SIA+SIV</i>	2025	2025	2024	2.05	0.52	2.93	2022	2023	2027	2029
<u>SSP2 4.5</u>										
<i>SIA+SIE</i>	2038	2039	2040	4.54	-0.12	2.70	2030	2034	2042	2045
<i>SIA+SIT</i>	2035	2035	2036	3.56	-0.26	2.78	2029	2032	2038	2040
<i>SIA+SIV</i>	2026	2025	2025	2.28	0.55	3.12	2022	2024	2028	2030
Time trend										
<i>SIA+SIE</i>	2038	2037	2036	5.80	0.79	4.11	2029	2033	2042	2048
<i>SIA+SIT</i>	2033	2032	2032	4.00	0.57	4.23	2027	2029	2036	2040
<i>SIA+SIV</i>	2028	2028	2027	3.43	0.79	4.06	2023	2025	2031	2034

Notes: We show summary statistics for distributions of first NIFA years for linear carbon-trend and quadratic time-trend constrained bivariate models. Std is standard deviation, skew is skewness, kurt is kurtosis, and xx% is the xx-th percentile. All years are rounded to the nearest integer.

and *SIA+SIV*, respectively. The projected first-NIFA year range is 2041-2031=10 years. The mean projected first-NIFA year is 2036, the same as with the earlier carbon-trend projections.

All told, the point forecasts of first-NIFA years from the carbon-trend models and the direct time-trend models are in striking agreement: NIFA will arrive very soon. We now proceed to provide a more complete characterization of the uncertainty surrounding the first-NIFA point forecasts, via a full accounting of first-NIFA probability distributions.

5 Probabilistic Assessment of Sea Ice Disappearance

Here we maintain our focus on first-NIFA years, but we build up approximations to their full probability distributions. Unlike our earlier first-NIFA point projections, which are based

simply on extrapolated deterministic trends, here we account for random variation, which lets us learn not only about central tendencies of the first-NIFA distributions (mean, median, mode), but also other moments and related statistics (standard deviation, skewness, kurtosis, left- and right-tail percentiles, etc.)

Results appear in Table 2, based on both bivariate carbon-trend models (for the emissions scenarios SSP5 8.5, SSP3 7.0, and SSP2 4.5) and direct time-trend models. Let us start with the measures of central tendency of the first-NIFA year distribution. It is immediately clear that – regardless of carbon-trend vs direct time trend, regardless of SSP scenario for the carbon trends, and regardless of the indicator blended with *SIA* – NIFA will arrive relatively soon, precisely as indicated in our first-NIFA projections based on deterministic extrapolations. Indeed the central tendencies of the distributions of NIFA years in Table 2 are generally a bit *earlier* than the corresponding years in Table 1. For example, for the leading baseline case, carbon trend *SIA+SIT* using mid-range emissions scenario SSP3 7.0, the distribution median is 2033, a bit earlier than the 2036 reported in Table 1.

The slightly earlier central tendencies of NIFA arrival in Table 2 occur because, when simulating sample pathways, the addition of stochastic shocks to a declining deterministic trend, particularly one concave to the origin (such as ours), might shorten the time necessary to achieve a given threshold. The random variation raises the possibility of a transitory fall below the threshold even before the deterministic trend achieves it on a sustained basis.¹² We call this the “principle of stochastic precedence”.¹³ The discrepancy between the timing of the deterministic first NIFA year and the mean (or median or mode) of the stochastic first NIFA year depends on the curvature of the trend and the variance of the shocks. A steeper slope, a more concave trend curve, or a smaller error variance will reduce the timing difference.

Let us now discuss the right tails of the NIFA arrival distributions. Consider again the leading baseline case: carbon trend *SIA+SIT* with mid-high emissions scenario SSP3 7.0. The “80%” column of Table 2 reports an eighty percent chance of first NIFA by 2036, and this “NIFA will arrive very soon” projection is robust to the modeling strategy (carbon trend, direct time trend), the sea ice indicator variables blended with *SIA* (*SIE*, *SIT*, *SIV*), emissions assumptions (SSP5 8.5, SSP3 7.0, SSP2 4.5), and confidence levels (80%,

¹²Consider, for example, a gentle deterministic trend that slowly approaches zero from above. This series will continue to run just above zero for a while before hitting zero. Adding random shocks to that trend, on the other hand, will almost certainly push the series below zero considerably sooner.

¹³According to the simulation, stochastic shocks are more likely to result in early NIFA years (79.85%) than later NIFA years (9.51%).

95%). Even the most extreme late arrival (moving up and down the 80%” column) is quite soon (2042), and the most extreme early arrival is 2027! Returning to the baseline case but increasing the confidence level from 80% all the way to 95% increases the NIFA arrival year by only two years – from 2036 to 2038. Alternatively, maintaining the 80% confidence level but moving to the optimistic lower emissions scenario SSP2 4.5 again postpones NIFA arrival by only two years.

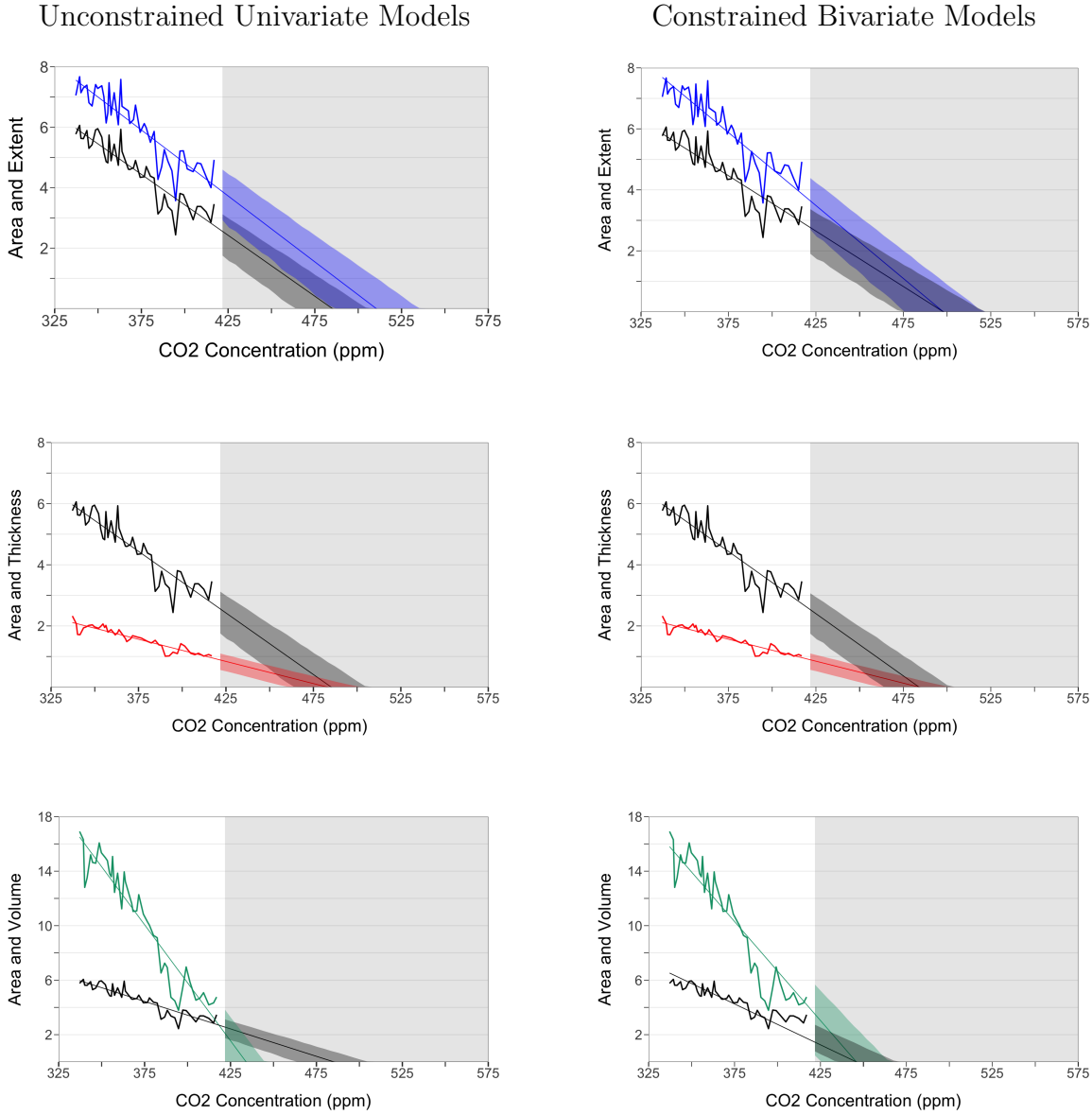
6 Carbon Trends Using Atmospheric Concentration

In Section 4, we checked the robustness of our carbon-trend results by comparing them to directly fitted time trends. In this section, we implement a second major robustness check by reexamining the carbon-trend estimates and forecasts using the atmospheric CO₂ concentration (measured in parts per million, ppm) as a different measure of cumulative CO₂.¹⁴ Although CO₂ emissions data are widely used for estimate the Arctic climate sensitivity Notz and Stroeve (2016), atmospheric CO₂ concentration has several advantages as a measure of carbon for this purpose. First, it is the most relevant metric for assessing the amount of heat-trapping gasses in the atmosphere, which is the source of global warming and Arctic ice melt. Furthermore, atmospheric concentration accounts for global carbon absorption. As the efficacy of natural terrestrial and oceanic carbon sinks changes and CO₂ absorption rates vary over time, concentration will better capture the extent to which greenhouse gases are driving climate change. Finally, atmospheric CO₂ concentration is less subject to measurement error. Fossil CO₂ emission estimates are indirectly based on energy, fuel use, and cement production data, while emissions from land-use changes are based on deforestation calculations. By contrast, atmospheric concentration is measured by direct air sampling.

The concentration-based carbon-trend results appear in Figure 5 (carbon trends in ice-carbon space) and Figure 6 (implied carbon trends in ice-time space), which are very similar in appearance to the earlier results based on cumulative emissions (compare to Figures 2 and 3). Importantly, a linear carbon trend for atmospheric concentration appears to fit well for each measure of Arctic sea ice. Across the panels of Figure 5, the projected atmospheric concentration CO₂ at first *SIA* IFA is generally on the order of 480 to 500 ppm. The corresponding CO₂ for first NIFA is 465 ppm, which when compared to the current CO₂ level of about 415 ppm puts the carbon budget at around 50 ppm for reaching an effectively ice-free Arctic Ocean.

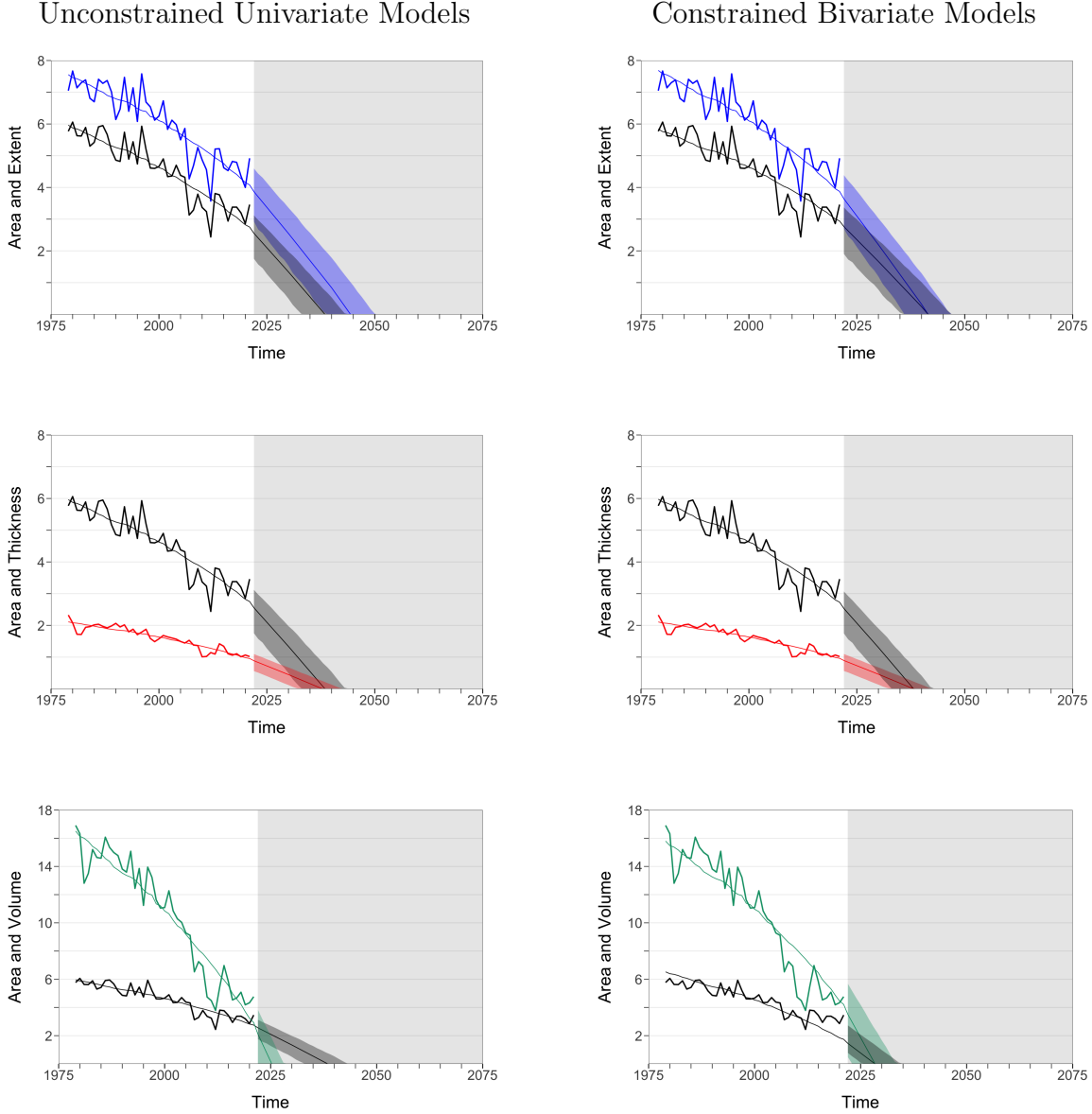
¹⁴For data source and details, see Appendix A.

Figure 5: September Arctic Sea Ice Indicators:
 Estimated Linear Carbon Trends in Ice-Carbon Space Under *SSP3 7.0*
 CO_2 Measured as Atmospheric Concentration



Notes: Each panel displays a pair of sea ice indicators graphed against CO_2 (atmospheric global carbon dioxide concentration, measured in ppm). We show extent in blue (measured in 10^6 km^2), area in black (measured in 10^6 km^2), thickness in red (measured in m), and volume in green (measured in 10^6 km^3). In the univariate column, we show linear carbon-trend fits and projections based on Equation (3). In the bivariate column, we show linear carbon-trend regression fits and forecasts constrained to reach zero simultaneously, based on Equation (4). The historical sample period (unshaded) is 1979-2021, and the projection intervals obtained by simulation have 90% coverage.

Figure 6: September Arctic Sea Ice Indicators:
 Estimated Linear Carbon Trends in Ice-Time Space Under *SSP3 7.0*
 CO_2 Measured as Atmospheric Concentration



Notes: Each panel displays a pair of sea ice indicators graphed against time. We show extent in blue (measured in 10^6 km^2), area in black (measured in 10^6 km^2), thickness in red (measured in m), and volume in green (measured in 10^6 km^3). In the univariate column, we show linear carbon-trend fits and forecasts based on Equation (3)), converted from ice-carbon space to ice-time space. In the bivariate column, we show linear carbon-trend regression fits and forecasts constrained to reach zero simultaneously, based on Equation (4), and again converted from ice-carbon space to ice-time space. The underlying CO_2 measure is atmospheric concentration, measured in ppm. The historical sample period (unshaded) is 1979-2021, and the projection intervals obtained by simulation have 90% coverage.

The implied projected first-IFA and first-NIFA years from the concentration-based carbon-trend regressions using the SSP3 7.0 scenario are shown in Figure 6. The univariate projected *SIA* first-IFA year is 2039, and the corresponding bivariate constrained projected first-IFA years are 2042, 2039, and 2029, depending on whether *SIA* is modeled jointly with *SIE*, *SIT*, or *SIV*, respectively. These are all several years earlier than the corresponding first-IFA years obtained using cumulative emissions.

The implied concentration-based first-NIFA probability distributions appear in Table 3. They are nearly identical in shape to the earlier-reported emissions-based first-NIFA distributions, with one difference: the concentration-based distribution is shifted slightly leftward relative to the emissions-based distribution (i.e., shifted toward earlier first-NIFA years). Using SSP3 7.0 and *SIA+SIT*, for example, produces a concentration-based median first NIFA of 2031, for example, in contrast to our earlier emissions-based 2033. The left-shifting of the concentration-based distribution makes its right tail thinner, so its 80th and 95th percentiles drop by even more relative to the emissions-based distribution. Moving from emissions to concentration lowers the 80th percentile from 2036 to 2033 (again using SSP3 7.0 and *SIA+SIT*) and lowers the 95th percentile from 2038 to 2034.

7 Conclusions and Directions for Future Research

We have constructed and compared projections of September Arctic sea ice. We prefer bivariate projections, because they enlarge the information set on which projections are based, in two ways. First, the bivariate projections blend the information in the history of *SIA* with that in the histories of other sea ice indicators, such as *SIE*, *SIT*, and *SIV*, which may improve projection accuracy. Second, they provide regularization by enabling us to constrain first IFA to coincide across sea ice indicators, thereby imposing appropriate geophysical constraints on otherwise flexible statistical models.

We ultimately produce full probability distribution projections of first-NIFA years, based on constrained bivariate models. Using cumulative carbon emissions data, the median of our preferred first-NIFA distribution is 2033, with 80% probability by 2036 and 95% probability by 2038. Using atmospheric CO₂ concentration data, the median is 2031, with 80% probability by 2033 and 95% probability by 2034. Therefore, it is very likely that the summer Arctic Ocean will be effectively ice-free at some time before the middle of the next decade.

The results are largely robust to the modeling strategy (univariate or multivariate, carbon trend or direct time trend), the sea ice indicator variable blended with *SIA* (*SIE*, *SIT*,

Table 3: September Arctic Sea Ice Indicators:
 Probability Distributions of *SIA* First September NIFA Years
 CO_2 Measured as Atmospheric Concentration

	Mean	Median	Mode	Std	Skew	Kurt	5%	20%	80%	95%
<u>SSP5 8.5</u>										
<i>SIA+SIE</i>	2032	2033	2033	2.79	-0.45	3.06	2027	2030	2035	2036
<i>SIA+SIT</i>	2030	2031	2031	2.34	-0.53	3.10	2026	2028	2032	2034
<i>SIA+SIV</i>	2024	2024	2024	1.63	0.59	3.01	2022	2023	2026	2027
<u>SSP3 7.0</u>										
<i>SIA+SIE</i>	2033	2033	2034	3.08	-0.30	2.92	2027	2030	2035	2037
<i>SIA+SIT</i>	2031	2031	2031	2.47	-0.40	3.07	2026	2029	2033	2034
<i>SIA+SIV</i>	2024	2024	2024	1.67	0.60	3.04	2022	2023	2026	2027
<u>SSP2 4.5</u>										
<i>SIA+SIE</i>	2037	2037	2038	4.20	-0.17	2.70	2029	2033	2040	2043
<i>SIA+SIT</i>	2034	2034	2035	3.33	-0.33	2.91	2028	2031	2037	2039
<i>SIA+SIV</i>	2025	2025	2025	2.16	0.57	3.10	2022	2023	2027	2029
<u>Time trend</u>										
<i>SIA+SIE</i>	2038	2037	2036	5.80	0.79	4.11	2029	2033	2042	2048
<i>SIA+SIT</i>	2033	2032	2032	4.00	0.57	4.23	2027	2029	2036	2040
<i>SIA+SIV</i>	2028	2028	2027	3.43	0.79	4.06	2023	2025	2031	2034

Notes: We show summary statistics for distributions of first NIFA years for linear carbon- and quadratic time-trend models. Std is standard deviation, skew is skewness, kurt is kurtosis, and xx% is the xx-th percentile. All years are rounded to the nearest integer.

SIV), emissions assumptions (SSP5 8.5, SSP3 7.0, SSP2 4.5), CO₂ measures (cumulative emissions, atmospheric concentration), and statistical confidence levels (80%, 95%). Hence there is no escaping the sharp bottom line: The Arctic will become seasonally ice free very soon – most likely in the early to mid-2030’s – even with successful global adoption of a lower emissions path.

As regards future research, it is of interest to assess whether the robust linear relationship between Arctic *SIA* and carbon dioxide, which we have documented in the observational record and used to make probabilistic assessments of NIFA arrival, is also present in simulated paths from large-scale dynamical climate models. If so, it will be of great interest to assess whether the climate sensitivity – the parameter b in our Equation (3) – embedded in the large-scale models is sufficiently strong to achieve consistency with the rapid observed historical Arctic sea ice diminution, and our projected continued rapid diminution. Diebold and Rudebusch (2022a) take steps toward that goal.

Appendices

A Data

The data are annual September Arctic sea ice area, extent, thickness, and volume, 1979-2021.

Area data are from the National Snow and Ice Data Center (Sea Ice Index monthly dataset, Version 3, Dataset ID G02135, <https://nsidc.org/data/G02135/versions/3>). Area is from 30.98N, measured in 10^6 km^2 . The satellites miss the “pole hole”, and the published *SIA* data exclude it, implicitly assuming that the pole hole has zero ice ($c=0$). A better approximation is to assume that the pole hole has full ice ($c=1$). Hence we first fill the pole hole by adding $1.19 \times 10^6 \text{ km}^2$ to *SIA* from sample start through July 1987, $0.31 \times 10^6 \text{ km}^2$ from September 1987 through December 2007, and $0.029 \times 10^6 \text{ km}^2$ from January 2008 to present.¹⁵

Extent data are from the National Snow and Ice Data Center (Sea Ice Index monthly dataset, Version 3, Dataset ID G02135, <https://nsidc.org/data/G02135/versions/3>). Extent is from 30.98N, measured in 10^6 km^2 .

Thickness and volume date are from PIOMAS at the Polar Science Center, <http://psc>.

¹⁵See the NSIDC Sea Ice Index Version 3 User Guide, <https://nsidc.org/data/G02135/versions/3>, p. 17.

apl.uw.edu/research/projects/arctic-sea-ice-volume-anomaly/data/. Thickness is from 49N, measured in m, where greater than 0.15 m. Volume is from 49N, measured in 10^3 km^3 . Volume data are published monthly. Thickness data are published on daily (file PIOMAS.thick.daily.1979.2020.Current.v2.1-2.dat), and we transform the daily data into monthly averages.

Cumulative CO₂ emissions data are taken from Rogelj et al. (2021) and the corresponding IPCC report (Allan et al., 2022). The actual dataset (Rogelj et al., 2021) is at https://data.ceda.ac.uk/badc/ar6_wg1/data/spm/spm_10/v20210809. From the latter, we use the following files:

1. *Top_panel_HISTORY.csv*,
2. *Top_panel_SSP2-45.csv*,
3. *Top_panel_SSP3-70.csv*,
4. *Top_panel_SSP5-85.csv*.

We merge annual historical cumulative emissions for the period 1850-2019 with data from each of the three scenarios (SSP2 4.5, SSP3 7.0, SSP5 8.5) from 2020 until 2100. This leaves us with three annual time series 1850-2100, with a common historical part 1850-2019.

The historical (1979-2021) CO₂ atmospheric concentration data (in parts per million, PPM) are taken from NOAA Global Monitoring Laboratory ¹⁶ CO₂ is measured at Mauna Loa Observatory, Hawaii.

Data for the period 2022-2100 are taken from the SSP Public Database (Version 2.0) (<https://tntcat.iiasa.ac.at/SspDb>). The individual scenarios are retrieved as follows: Data for the SSP2 4.5 scenario are based on the *MESSAGE-GLOBIOM - SSP2-45* model with variable ID *Diagnostics—MAGICC6—Concentration—CO2* for region *World*. Data for the SSP3 7.0 scenario are based on the *AIM/CGE - SSP3-Baseline* model with variable ID *Diagnostics—MAGICC6—Concentration—CO2* for region *World*. Data for the SSP5 8.5 scenario are based on the *REMIND-MAGPIE - SSP5-Baseline* model with variable ID *Diagnostics—MAGICC6—Concentration—CO2* for region *World*. All three scenarios are composed of eleven data points between 2005 and 2100. Missing data points for the years 2022-2100 were filled by linear interpolation.

¹⁶See: https://gml.noaa.gov/webdata/ccgg/trends/co2/co2_mm_mlo.txt. The data file was created on 11/05/2021 at 10:28:56. The data were retrieved on 11/23/2021. Our calculations are based on the *de-seasonalized* data column.

B Details of Bootstrap Simulation

Our bivariate bootstrap projection interval simulation procedure, of which our univariate procedure is a special case, proceeds as follows at bootstrap replication i . First we estimate the model and collect residuals. Second, we draw pairs of those residuals, to preserve their cross-correlation, and we add them back to the in-sample fitted values. Third, we re-estimate the model on this synthetic data and use the re-estimated model to project out-of-sample. Finally, we draw pairs of residuals and add them to the forecasted paths to get the simulated path realizations. We repeat this for $i = 1, 2, \dots, 1000$. We then sort the simulated path values at each date and obtain the 90% intervals shown in Figure 4, with left and right endpoints given by the fifth and ninety-fifth percentiles, respectively, of the simulated path values.

Our bivariate bootstrap first NIFA simulation proceeds identically, with one extra step. At the end, once the simulated path realizations are in hand, we calculate the corresponding simulated first NIFA realizations, NIFA_i , $i = 1, 2, \dots, 1000$. We then obtain the first NIFA densities shown in Figure 4 by applying a nonparametric kernel density estimator to NIFA_i , $i = 1, 2, \dots, 1000$.

References

Allan, R.P., E. Hawkins, N. Ballouin, and B. Collins (2022), “IPCC, 2021: Summary for Policymakers,” In Masson-Delmotte, V., P. Zhai, A. Pirani, S.L. Connors, C. Péan, S. Berger, N. Caud, Y. Chen, L. Goldfarb, M.I. Gomis, M. Huang, K. Leitzell, E. Lonnoy, J.B.R. Matthews, T.K. Maycock, T. Waterfield, O. Yelekçi, R. Yu, and B. Zhou, eds., *Climate Change 2021: The Physical Science Basis. Contribution of Working Group I to the Sixth Assessment Report of the Intergovernmental Panel on Climate Change*, Cambridge University Press, in press. https://ipcc.ch/report/ar6/wg1/downloads/report/IPCC_AR6_WGI_SPM_final.pdf.

Alvarez, J., D. Yumashev, and G. Whiteman (2020), “A Framework for Assessing the Economic Impacts of Arctic Change,” *Ambio*, 49, 407–418.

Arias, P.A. et al. (2022), “Technical Summary,” In Masson-Delmotte, V., P. Zhai, A. Pirani, S.L. Connors, C. Péan, S. Berger, N. Caud, Y. Chen, L. Goldfarb, M.I. Gomis, M. Huang, K. Leitzell, E. Lonnoy, J.B.R. Matthews, T.K. Maycock, T. Waterfield, O. Yelekçi, R. Yu, and B. Zhou, eds., *Climate Change 2021: The Physical Science Basis. Contribution of Working Group I to the Sixth Assessment Report of the Intergovernmental Panel on*

Climate Change, Cambridge University Press, in press. https://www.ipcc.ch/report/ar6/wg1/downloads/report/IPCC_AR6_WGI_TS.pdf.

Bunzel, F., D. Notz, and L.T. Pedersen (2018), “Retrievals of Arctic Sea-Ice Volume and its Trend Significantly Affected by Interannual Snow Variability,” *Geophysical Research Letters*, 45, 11751–11759.

Chevallier, M., G.C. Smith, F. Dupont, J.F. Lemieux, G. Forget, Y. Fujii, F. Hernandez, R. Msadek, K.A. Peterson, A. Storto, and T. Toyoda (2017), “Intercomparison of the Arctic Sea Ice Cover in Global Ocean-Sea Ice Reanalyses From the ORA-IP Project,” *Climate Dynamics*, 49, 1107–1136.

Cooley, S.W., J.C. Ryan, L.C. Smith, C. Horvat, B. Pearson, B. Dale, and A.H. Lynch (2020), “Coldest Canadian Arctic Communities Face Greatest Reductions in Shorefast Sea Ice,” *Nature Climate Change*, 10, 533–538.

Diebold, F.X. and G.D. Rudebusch (2022a), “Climate Models Underestimate the Sensitivity of Arctic Sea Ice to Carbon Emissions,” Work in Progress, University of Pennsylvania.

Diebold, F.X. and G.D. Rudebusch (2022b), “Probability Assessments of an Ice-Free Arctic: Comparing Statistical and Climate Model Projections,” *Journal of Econometrics*, in press.

Fox-Kemper, B., H.T. Hewitt, C. Xiao, G. Adalgeirsdottir, S.S. Drijfhout, T.L. Edwards, N.R. Golledge, M. Hemer, R.E. Kopp, G. Krinner, A. Mix, D. Notz, S. Nowicki, I.S. Nurhati, L. Ruiz, J-B. Sallée, A.B.A. Slangen, and Y. Yu (2022), “Ocean, Cryosphere and Sea Level Change,” In Masson-Delmotte, V., P. Zhai, A. Pirani, S.L. Connors, C. Péan, S. Berger, N. Caud, Y. Chen, L. Goldfarb, M.I. Gomis, M. Huang, K. Leitzell, E. Lonnoy, J.B.R. Matthews, T.K. Maycock, T. Waterfield, O. Yelekçi, R. Yu, and B. Zhou, eds., *Climate Change 2021: The Physical Science Basis. Contribution of Working Group I to the Sixth Assessment Report of the Intergovernmental Panel on Climate Change*, Cambridge University Press, in press. https://ipcc.ch/report/ar6/wg1/downloads/report/IPCC_AR6_WGI_SPM_final.pdf.

Jahn, A., J.E. Kay, M.M. Holland, and D.M. Hall (2016), “How Predictable is the Timing of a Summer Ice-Free Arctic?” *Geophysical Research Letters*, 43, 9113–9120.

Johannessen, O.M. (2008), “Decreasing Arctic Sea Ice Mirrors Increasing CO₂ on Decadal Time Scale,” *Atmospheric and Oceanic Science Letters*, 1, 51–56.

Labe, Z., G. Magnusdottir, and H. Stern (2018), “Variability of Arctic Sea Ice Thickness Using PIOMAS and the CESM Large Ensemble,” *Journal of Climate*, 31, 3233–3247.

Leppäranta, M., V.P. Meleshko, P. Uotila, and T. Pavlova (2020), “Sea Ice Modelling,” In Johannessen, O.M., Bohylev, L.P., Shalina, E.V., and Sandven, S., eds., *Sea Ice in the Arctic: Past Present and Future*, 318–388, Springer Nature.

Matthews, D.H., K.B. Tokarska, J. Rogelj, C.J. Smith, A.H. MacDougall, K. Haustein, N. Mengis, S. Sippel, P.M. Forster, and R. Knutti (2021), “An Integrated Approach to Quantifying Uncertainties in the Remaining Carbon Budget,” *Communications Earth & Environment*, 2, 7.

Mudryk, L.R., J. Dawson, S.E.L. Howell, C. Derksen, T.A. Zagon, and M. Brady (2021), “Impact of 1, 2 and 4°C of Global Warming on Ship Navigation in the Canadian Arctic,” *Nature Climate Change*, 11, 673–679.

Notz, D. and J. Stroeve (2016), “Observed Arctic Sea-Ice Loss Directly Follows Anthropogenic CO₂ Emission,” *Science*, 354, 747–750.

Notz, D. et al. (2020), “Arctic Sea Ice in CMIP6,” *Geophysical Research Letters*, 47, e2019GL086749.

Rogelj, J., B. Trewin, K. Haustein, P. Canadell, S. Szopa, S. Milinski, J. Marotzke, and K. Zickfeld (2021), “Summary for Policymakers of the Working Group I Contribution to the IPCC Sixth Assessment Report - Data for Figure SPM.10 (v20210809),” NERC EDS Centre for Environmental Data Analysis.

Rosenblum, E. and I. Eisenman (2017), “Sea Ice Trends in Climate Models Only Accurate in Runs with 49 Biased Global Warming,” *Journal of Climate*, 30, 6265–6278.

Schweiger, A., R. Lindsay, J. Zhang, M. Steele, H. Stern, and R. Kwok (2011), “Uncertainty in Modeled Arctic Sea Ice Volume,” *Journal of Geophysical Research: Oceans*, 116, C00D06.

Schweiger, A.J., S. Michael, J. Zhang, G.W.K. Moore, and K.L. Laidre (2021), “Accelerated Sea Ice Loss in the Wandel Sea Points to a Change in the Arctic’s Last Ice Area,” *Communications Earth & Environment*, 2, 1–11.

Selyuzhenok, V., I. Bashmachnikov, R. Ricker, A. Vesman, and L. Bobylev (2020), “Sea Ice Volume Variability and Water Temperature in the Greenland Sea,” *The Cryosphere*, 14, 477–495.

Shalina, E.V., O.M. Johannessen, and S. Sandven (2020a), “Changes in Arctic Sea Ice Cover in the Twentieth and Twenty-First Centuries,” In Johannessen, O.M., Bohylev, L.P., Shalina, E.V., and Sandven, S., eds., *Sea Ice in the Arctic: Past Present and Future*, 93–166, Springer Nature.

Shalina, E.V., K. Khvorostovsky, and S. Sandven (2020b), “Arctic Sea Ice Thickness and Volume Transformation,” In Johannessen, O.M., Bohylev, L.P., Shalina, E.V., and Sandven, S., eds., *Sea Ice in the Arctic: Past Present and Future*, 167–246, Springer Nature.

Stroeve, J. and D. Notz (2018), “Changing State of Arctic Sea Ice Across All Seasons,” *Environmental Research Letters*, 13, 103001.

Stroeve, J.C., M.C. Serreze, M.M. Holland, J.E. Kay, J. Malanik, and A.P. Barrett (2012), “The Arctic’s Rapidly Shrinking Sea Ice Cover: A Research Synthesis,” *Climatic Change*, 110, 1005–1027.

Wang, Lei, Xiaojun Yuan, Mingfang Ting, and Cuihua Li (2016), “Predicting Summer Arctic Sea Ice Concentration Intraseasonal Variability Using a Vector Autoregressive Model,” *Journal of Climate*, 29, 1529–1543.

Wang, M. and J.E. Overland (2009), “A Sea Ice Free Summer Arctic Within 30 Years?” *Geophysical Research Letters*, 36, L07502.

Zhang, J. and D.A. Rothrock (2003), “Modeling Global Sea Ice with a Thickness and Enthalpy Distribution Model in Generalized Curvilinear Coordinates,” *Monthly Weather Review*, 131, 845–861.

Zygmuntowska, M., P. Rampal, N. Ivanova, and L.H. Smedsrød (2014), “Uncertainties in Arctic Sea Ice Thickness and Volume: New Estimates and Implications for Trends,” *The Cryosphere*, 8, 705–720.